**Shaowu Bao[1], Leonard Pietrafesa[1], Paul Gayes[1], Stephen Noble[2], Brian Viner[2], Jian-Hua Qian[2], David Werth[2], Grant Mitchell[1], Savannah Burdette[1]**

[1]Coastal Carolina University.

[2]Savanna River National Laboratory.

Corresponding author: Shaowu Bao (`sbao@coastal.edu`)

Key Points:

- The combination of surface reanalysis and remote sensing data can be used to map the spatial distribution of sea breeze winds.
- In the southeastern United States 63 percent of the days experienced sea breezes from March to September 2019. Sea breezes increase from March to July and then decrease to September.
- Sea breeze winds leave footprints in a band parallel to the coastline up to about 220 km inland, after which the sea breeze winds quickly diminish. The mapping results are consistent with model simulations and theoretical estimate.

Abstract

Sea breeze winds are observed at various locations worldwide, but the spatially continuous mapping of sea breeze winds is rare. We have developed a scheme to map the areas of the southeastern United States (US) coast influenced by sea breeze winds using a range of surface re-analysis data to identify their occurrence. Changes in wind direction and dew point temperature are both used to detect a potential sea breeze signature, which is then confirmed by cumuliform clouds seen in satellite images or coastal fronts shown as cohesive lines in radar reflectivity images. Filters are employed to remove onshore winds not induced by the temperature difference between land and sea.

From March to September 2019, this scheme identified 134 days with sea breeze occurrence somewhere in the southeastern US, a frequency of 63 percent.. The number of sea breezes increased from March to July and then decreased to September. Deep inland propagation of sea breezes during this period left footprints in a band parallel to the coastline up to about 220 km inland, after which the sea breeze winds quickly diminished. Comparisons show that the findings using the scheme are consistent with site observations, theoretical estimates, and idealized and semi-idealized numerical model simulations.

**Plain Language Summary**

A sea breeze is a wind that starts to blow from the ocean toward land during the late afternoon and can last into late evenings, nights and into early morning. It is caused by the difference in temperature between the land and the water. A sea breeze is an important weather phenomenon along the coast that moves cold, moisture laden sea air masses and particles inland and can cause rainstorms.

Data sets from various coastal locations all over the world show sea breeze winds and how they move inland, but it is rare to map the sea breeze winds' spatial distribution because of a general lack of continuous in-situ weather data. In this study, we use a high-resolution near-surface wind and moisture model product along with satellite and radar images to find the locations that sea breeze winds reach onshore. This method was tested to find sea breeze wind locations in the southeastern US from March to September 2019. The results show that during this period sea breezes occurred 63 percent of the days somewhere in the southeastern US. Sea breezes increased From March to July, and then decreased thereafter. When sea breezes moved inland during this period, the summation of them results in a trail in a band that runs parallel to the coast for up to around 220 km inland. After that, the sea breeze winds disappear. When compared, the scheme's results are in line with in-situ observations, theoretical estimates, and idealized and semi-idealized model simulations.

## 1 Introduction

A sea breeze is a mesoscale wind circulation that occurs along coastal areas worldwide when winds blow from a large body of water, such as an ocean or a large lake, toward or onto land (Miller et al. 2003; Simpson 1994). The sea breeze is an important coastal weather phenomenon that transports cold, moist sea air masses inland, causes convective storms, and has the potential to impact air quality near the Earth's surface. The fundamental mechanism of sea breeze propagation is relatively well established - it is thermally driven by the temperature difference between land and sea and the resulting pressure gradient force (Schwartz 2006). Pearce (1955) was the first to conclude that Coriolis-induced rotation ultimately limits inland motion of the sea breeze. Furthermore, Rotunno (1983) used a set of simplified linear motion equations to derive and estimate the maximum extent of mid- and high-latitude (latitude $> 30^{o}$) sea breeze inland propagation near the ground as a function of latitude (and hence Coriolis effect), atmospheric stability, and the vertical motion scale. Rotunno (1983) also concluded that the sea breeze is in the form of internal waves that extend an "infinite" distance inland for regions with latitudes less than $30^{o}$. The sea breeze is entirely limited by friction at the equator, where the Coriolis force is zero. The above equation implies that Coriolis force and atmospheric stability are the only two factors that determine the extent of sea breeze inland propagation.

However, factors other than Coriolis force and atmospheric stability can influence the propagation of sea breezes (Arritt 1993, Miller et al. 2003, Wermter et al. 2021), such as land-sea temperature difference, inland temperature gradient, coastline shape, topography, land type and friction, and prevailing winds, as well as interaction with other mesoscale systems. As a result, the characteristics of sea breeze propagation established in one area may not be accurate in other regions. The interaction of land, water, and atmosphere creates a complex sea breeze system in the Southeastern United States (SEUS), influencing clouds, convection, and precipitation. Coastal sea breeze penetration is a major

feature in this area that supports convection in the SEUS via associated lifting and the transport of marine aerosols to inland regions. In terms of the interactions between aerosols, clouds, convection, and precipitation, the SEUS is an understudied region, and it is critical that we understand how to identify and characterize the inland penetrating sea breeze and how it interacts with other atmospheric phenomena.

Sea breezes have several distinct characteristics that can be used to detect their occurrence. Studies have been conducted over the last 40 years to determine the best method for identifying the occurrence of sea or lake breezes using station observational data from at least two sites (Viner et al. 2021; Borne et al. 1998; Laird et al. 2001; Papanastasiou et al. 2010; Ryznar and Touma 1981). Despite differences in strategies, all methods ultimately determine the likelihood of sea breezes based on key meteorological principles such as land-sea temperature contrast (McKendry and Roulet 1994), rapid changes in wind speed and directions from the synoptically driven wind to onshore sea breeze wind that are not caused by other synoptic weather events (Borne et al. 1998; Laird et al. 2001; Papanastasiou et al. 2010; Qian et al. 2021; Viner et al. 2021), increase in air humidity, and the signature patterns sea breeze fronts leave on remote sensing images.

Using these methods, inland propagation of the sea breeze has been extensively studied, and deep inland penetrations of the sea breeze have been observed at various locations all over the world. Deep inland penetration distances in low-latitude areas have been reported to reach 400 km in Australia (Garratt 1985) and Texas (Hu and Xue 2016), an average of 202 km with a range of [91, 372] km in the Red Sea (Khan et al. 2018), 200km in Australia (Simpson 1994), 150-200 km in Japan (Kondo 1990), 150 km at the Savannah river site (Buckley and Kurzeja 1997; Viner et al. 2021), 150 km at the coast of Oman (Charabi et al. 2013), 15km in Beaufort Sea coast of Alaska (Kozo 1982), 40km Lake breeze in Chicago (Lyons 1972), 60-80km in Indonesia (Hadi et al. 2002), 100 km in England (Simpson et al. 1977), 100km in Ontario, Canada (McKendry and Roulet 1994) and 150km in Southeastern Spain (Kottmeier et al. 2000).

However, because the majority of these works used individual observational sites, their conclusions are more local than regional. Strategies developed for one location may not work effectively in another due to local abnormalities such as the shoreline configuration and inland topography (Miller et al. 2003; Simpson 1994). As a result, while these studies can reveal the occurrence and characteristics of sea breezes at specific locations, they may not improve our understanding of sea breeze spatial distribution and the maximum distance of inland penetration, and thus cannot achieve the goal of studying sea breeze events at multiple scales due to a scarcity of observation data at regional scales like the SEUS. This limitation resulted in large uncertainties in the literature regarding the maximum extent of sea breeze inland propagation as seen above. The fact that a sea breeze is observed at one location does not rule out the possibility that it can pass that location and propagate further. There is no comprehensive under-

standing of the characteristics of sea breeze inland propagation for the SEUS region.

In this study, we present a method for detecting and mapping the occurrence and strength of sea breeze onshore winds by combining spatially continuous data sets, near surface atmospheric reanalysis, satellite imagery, and radar reflectivity imagery. An atmospheric reanalysis is a global model that recreates the atmospheric state variables evolution using interpolation methods, data assimilation from meteorological stations, satellites, upper air balloons, aircraft, and ships, among others, and the use of physics equations to consistently represent spatial and temporal atmospheric variability, resulting in a more realistic and consistent dataset. Because atmospheric reanalysis data is both temporally and spatially continuous, it overcomes the previously mentioned limitation of detecting sea breeze occurrence at individual locations. Another advantage of such an atmospheric reanalysis is the space–time consistency of the various meteorological variables required to detect sea breeze; thus, there is no need to address issues such as missing data, site relocation, and inhomogeneity that are frequently encountered when raw observational data is used.

The goal of this study is not only to identify sea breezes at discrete sites, but also to analyze the temporal and geographical characteristics of sea breezes, develop a sea-breeze fingerprint tool, and characterize their inland penetration over the SEUS region. The methods are portable and thus can be extended to other coastal regions. We develop the hypothesis that the previously mentioned sea breeze signatures observed at individual observational sites can also be detected in atmospheric reanalysis and remote sensing images, which will be tested by comparing the identified sea breeze occurrence with those from individual observational sites. Section 2 describes the data and the method of identification. Section 3 will present the results of the sea breeze mapping. In section 4, we conducted an idealized and a semi-idealized model simulations of sea breeze inland propagation in the SEUS region to provide a more in-depth understanding of the sea breeze inland propagation, and the simulation results are compared with the mapping results.

2 Data and Method

### 2.1 Description of Data

For our study, we chose three types of data that are both temporally and geographically continuous. The first is ERA5-Land, an enhanced global data set for the land component of the European Centre for Medium-Range Weather Forecasts (ECMWF) Reanalysis version 5 (ERA5) that provides a consistent view of the evolution of atmospheric variables over land over multiple decades at an enhanced resolution with a grid spacing of 9km (Muñoz-Sabater et al. 2021). ERA5-land provides global hourly surface temperature, dew point, and 10-m wind at a 9-km resolution, which are used in this study to objectively identify the onshore winds that indicate a sea breeze occurrence. This will be further confirmed by satellite and radar imagery, as described below. The

ERA5-Land data is obtained from the Google Earth Engine platform (https://developers.google.com/earth-engine/datasets).

The most recent generation of National Oceanic and Atmospheric Administration (NOAA) geostationary weather satellites, the Geostationary Operational Environmental Satellite-R Series (GOES-R) (Goodman et al. 2012), is used to confirm the presence of sea breezes. GOES satellites observe the Earth through 16 channels, including two visible channels as well as near infrared and infrared channels. The visible channels, with wavelengths of 0.47 um and 0.64 um, enable practically continuous daytime investigations of dust, haze, smoke, and clouds. In this study, we use the global hourly visible channel data at spatial grid spacing's ranging from 5km to 2km provided by GOES-R satellites. The distinctive cumuliform clouds in these GOES-R visible images that accompany the upward convective air motion when a sea breeze propagates inland from the coast are used to confirm sea breezes.

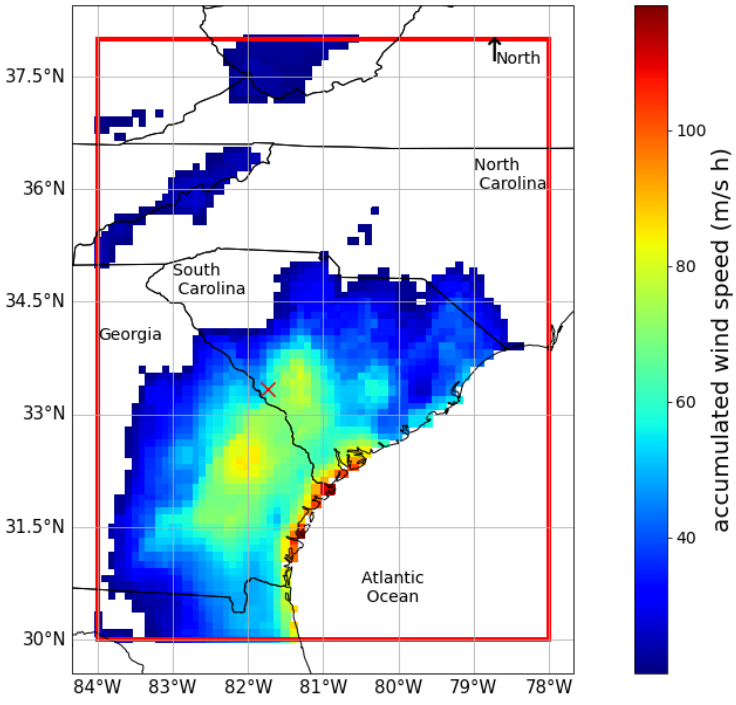


The National Weather Service (NWS) operates a network of 160 high-resolution S-band Doppler weather radars called NEXRAD (Next-Generation Radar), which are also used in this study to confirm the occurrence of sea breezes (https://www.ncei.noaa.gov/products/radar/next-generation-weather-radar). Koch and Ray (1997) examined the advantages and disadvantages of using Radar reflectivity imagery, GOES Satellite imagery, and conventional surface data to detect summertime convergence boundaries in North Carolina. They discovered that radar and satellite detected such boundaries in approximately

84% and 82% of the cases, respectively, whereas their surface observational stations revealed only 53% of the boundaries and detected 95 percent of all boundary lines when the satellite was used in conjunction with the radar. While a satellite and radar combination can be used to detect sea breezes, the goal of this study is to map the spatial footprint of sea breeze onshore winds. As a result, we employ the strategy of identifying onshore winds using ERA5-Land data and then confirming them with satellite and radar data.

### 2.2 Scheme

The study domain is depicted in Figure 1 as [30°N – 38°N, 84°W – 78°W]. The red cross near the border of SC and GA denotes the Savannah River Site (SRS), whose observations will be compared to this study's findings. The domain is divided into 5km x 5km mesh grid, and ERA5-land 10m wind and surface moisture data are interpolated to that mesh grid. Each day from March 1 to September 30, 2019, data is analyzed to identify grid points where a sea breeze occurrence has left a footprint. The local time has been adjusted so that the detection starts at noon each day and lasts 24 hours until noon the next day. This modification is required because it has been discovered (Viner et al. 2021) that a sea breeze that begins at the coast can often propagate inland overnight, reaching the SRS early the next morning. As a result, by combining the early morning cases with the afternoon cases from the previous day, the early morning cases will have more plausible traces of origin.

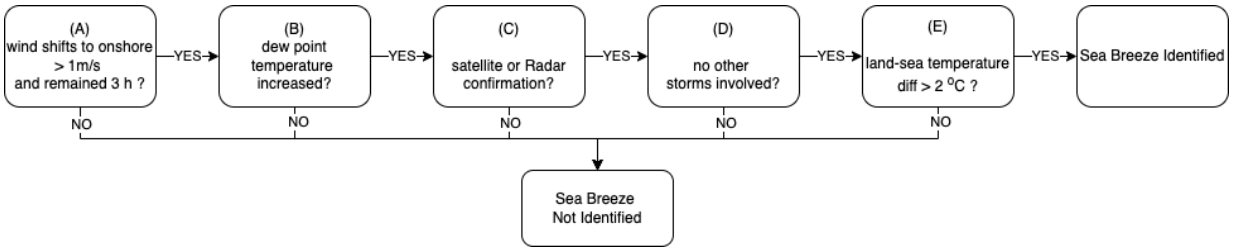


The flowchart of the scheme is shown in Figure 2. The objective algorithm searches domain points, one at a time, from the local time of 12 p.m. one day to 12 p.m. the next day, seeking grid locations that satisfy the following 2 criteria within the 24-hour period: i) The wind turns from whatever the prior synoptically driven wind was to sea breeze wind in the onshore direction and remains in that direction for at least 3 hours (Figure 2A), and ii) wind direction shifts must be accompanied by a rise in surface dew point temperature (Figure 2B). Considering the geometry of the Southeast United States' coastline in Figure 1: $\beta$ should be in the range of [270° – 360°], where $\beta$ is the wind direction that the winds blow to, 360 represents North and 270 represents West. Similar criteria have previously been used to detect sea breeze winds (Laird et al. 2001). Grid areas that match both requirements are thought to be likely influenced by the passage of sea source winds. This phase can be configured to run automatically and hence objectively, eliminating the need for human intervention. To illustrate the scheme: Figure 1 depicts these potential sea

breeze grid sites from 12pm on May 18 to 12pm on May 19, 2019, together with the average wind speed during the sea breeze effect. The colors in Figure 1 depict the daily cumulative hourly wind speed in meters per second (m/s h). A value of 10 m/s h at a specific grid point, for example, could be the result of a 10 m/s onshore wind speed lasting 1 hour or a 1 m/s onshore wind speed lasting 10 hours; thus, Figure 1 shows where the strongest onshore accumulated winds occurred during this sea breeze occurrence.

Following the objective automated detection of a sea breeze using ERA5-land data, visible light imagery from GOES-16 was used to confirm the presence of a sea breeze (Figure 2C). A cloud-free area along a coastline area along a coastline can be detected in satellite images as an inland propagating sea breeze, with mesoscale cumuliform clouds frequently present over land, indicating enhanced convection. The cloud-free belt along the coastline is where the sea breeze causes upward air motion but the air has not reached condensation levels. The initial sea breeze front can be seen from a line parallel to the coastline that separates cool, moist maritime air from warm, dry air over land. The Figure 3 depicts such cumuliform cloud bands in the demonstration case on the afternoon of May 18, 2019. These fair-weather cumulus clouds, the cloud-free belt near the coastline, and the distinctive boundary (blue line in Figure 3) between them form a well-documented sea breeze signature footprint (Simpson 1994).

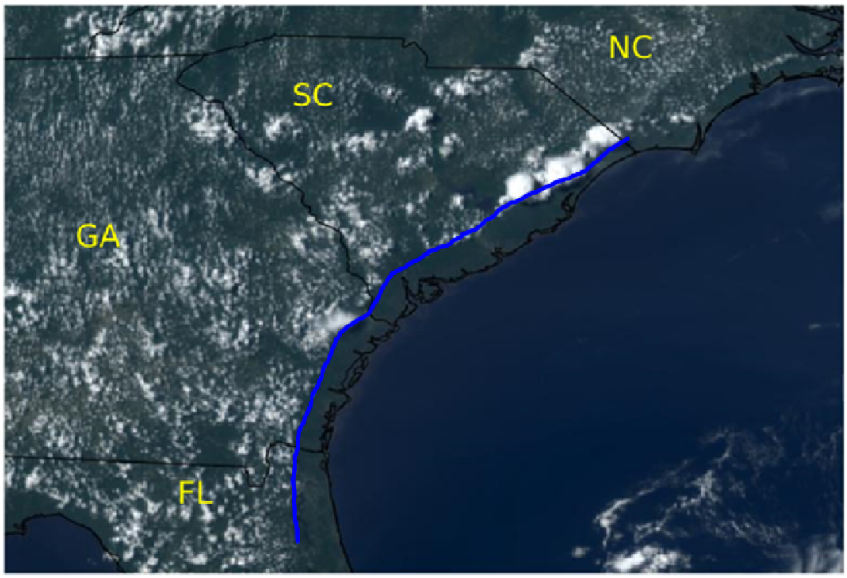

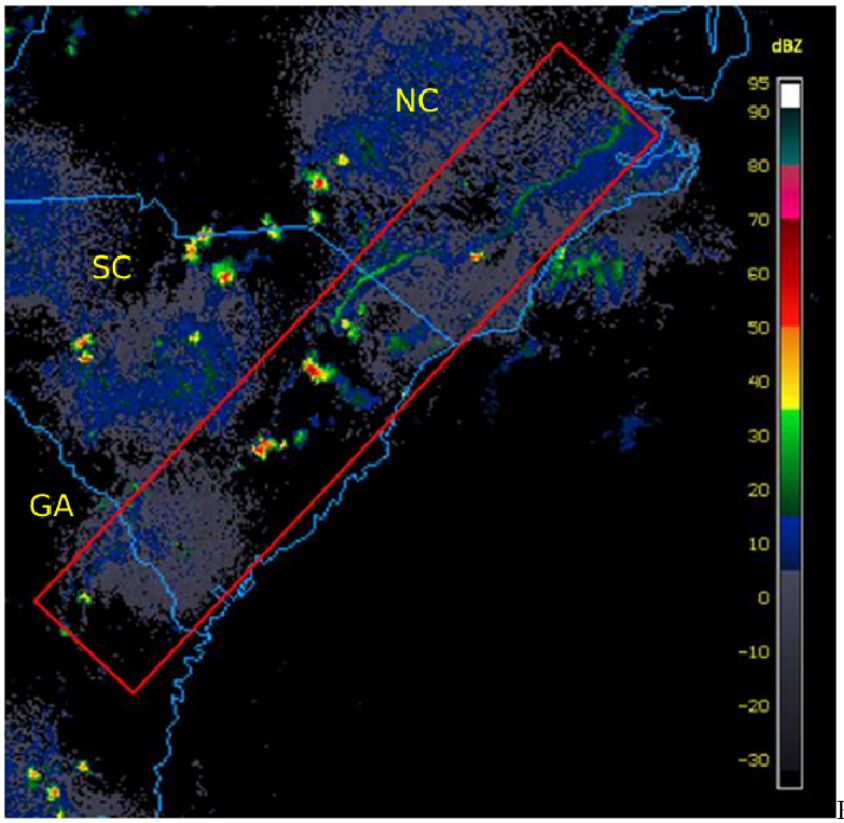


Radar data can also be used as an alternative source for confirming sea breezes (Figure 2C). Koch and Ray (1997) used radar to locate a linear area of relatively high reflectivity with a width of no more than 10 km to detect convective convergence boundaries, including those caused by sea breezes. A sea breeze is also confirmed in this study by a cohesive line of radar reflectivity that was roughly parallel to the coast and moving inland. Radar reflectivity for our demonstration case (Figure 4) shows a long line of high reflectivity extending from North Carolina to South Carolina during the late afternoon, indicating a frontal system. Low reflectivity values (dBZ 10 and negative dBZ values, depicted in blue and grey on Figure 4 indicate areas with very small hydrometeors. The coastal front depicted as the high reflectivity lines in Figure 4 was strong near the North Carolina (NC) and South Carolina (SC) border and weakened and lingered as it extended further into SC toward the southwest. This pattern was consistent with Figure 1 and Figure 3, which showed stronger onshore winds and larger areas of cumuliform clouds across the NC and SC border areas, respectively. Furthermore, the several high reflectivity areas in Figure 4 (inside the red rectangle) indicate stronger convections, and the locations of these strong convections are near the strong wind centers shown in Figure 1.

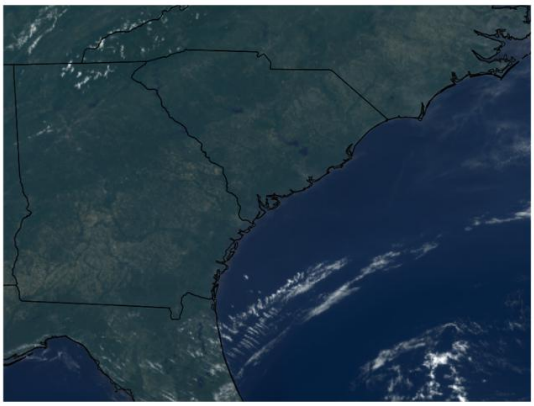

Two filters are then used as part of the sea breeze wind identification process to eliminate instances that met the above criteria but were not thermally driven. The first filter eliminates cases caused by synoptic-scale storms or hurricanes, as opposed to local thermal differences (Figure 2D). For example, there was no synoptic scale forcing the onshore wind on May 18, 2019 (Figure 5) as can be seen from the clear sky in the early afternoon preceding the onset of the sea breeze episode. Therefore, we can conclude that the onshore winds on May 18, 2019, were due to a sea breeze. The second filter utilizes the difference in temperature between land and sea (Figure 2E). In the demonstration case, on the afternoon of 18 May 2019 along the South Carolina and Georgia coasts, the coastal ocean water temperature averaged 24 °C and the land surface air temperature reached as high as 30 °C (not shown), a 6 °C difference, sufficient to generate a pressure gradient that drives the sea breeze. If the land temperature is cooler than or not warmer than the seawater temperature by at least 2 °C, any onshore winds, if present, are not considered thermally driven, and the day is removed from the detected sea breeze situations.

3 Results and Discussion

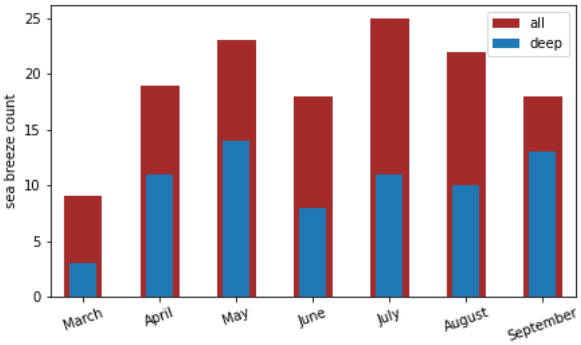


### 3.1 Case counts and temporal frequency

Although this study focuses on mapping the spatial footprint of sea breeze winds, the results provide an opportunity to also examine the temporal frequency of sea breeze events in the SEUS. Figure 6 depicts a monthly histogram of all sea breeze occurrences (red) and those that penetrated inland in the southeastern United States (cyan). From 03/01/2019 to 09/30/2019, 70 sea breeze events were detected as penetrating inland, while 64 were confined to a distance close (<20km) to the coast. We also see a cycle (Figure 6) of increasing sea breezes from March to July, followed by a decrease, except for June, when sea breezes are significantly lower than in the preceding and subsequent months. It is unknown if the exception was a one-time occurrence or if there are additional underlying causes.

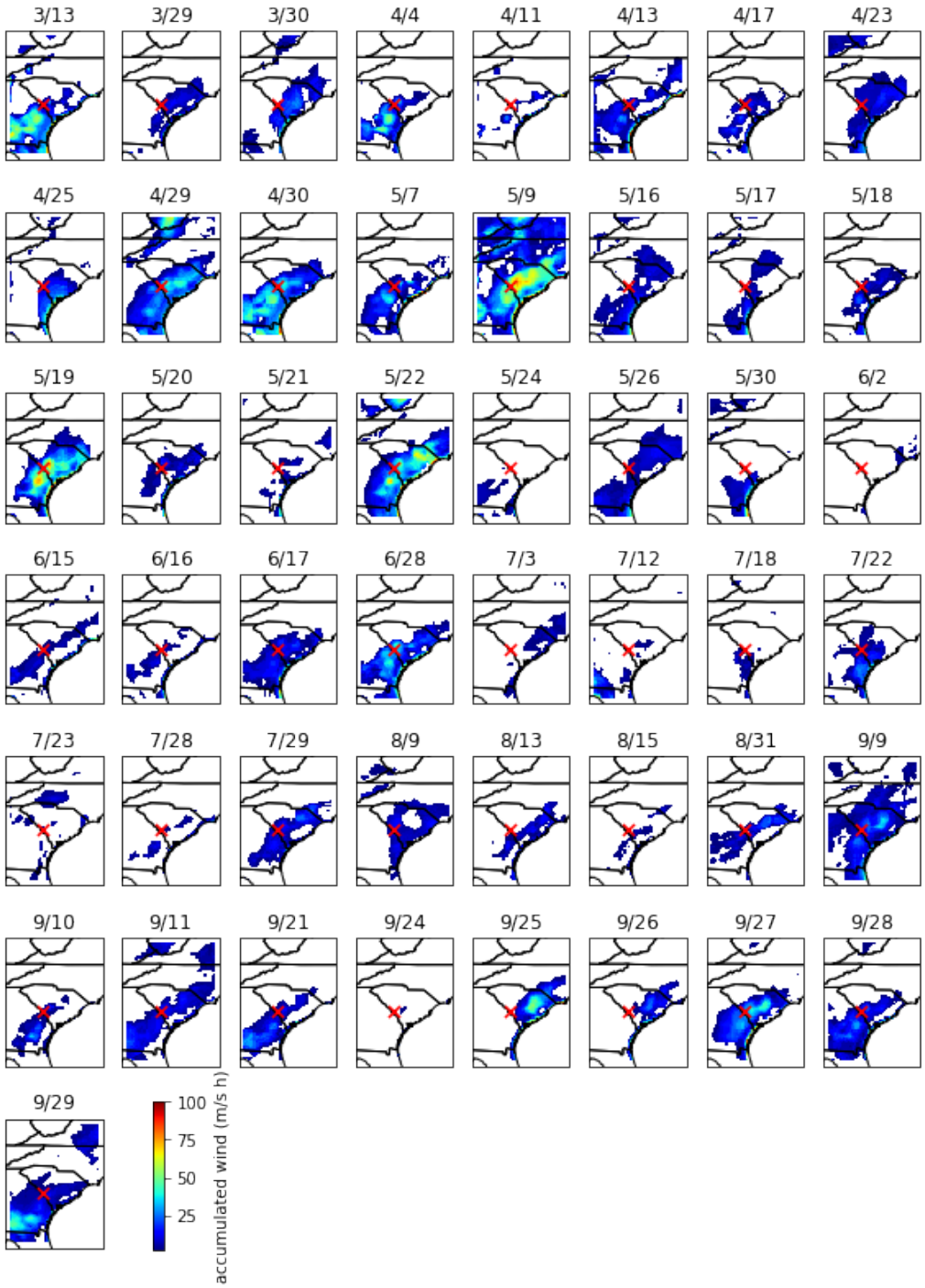


The frequency of sea breeze from March to September is 63%, close to the findings

of Hughes and Veron (2018), Khan et al. (2018), and Azorin-Molina and Lopez-Bustins (2008). Viner et al. (2021) utilized wind observations and a visual inspection of radar images to determine the impact of the sea breeze at the SRS (red cross in Figure 1). We compared the sea breeze occurrence identified by this study at the SRS location with those identified by Viner et al. (2021) to verify the robustness of both studies' methods.

From March to September 2019, Viner et al. (2021) identified 49 days with sea breeze occurrence. The method used in this work detected 41 of these 49 cases (Figure 7), yielding a probability of detection (POD) of $41/49 = 84\%$. Viner et al. recorded sea breezes at SRS on the following dates: 05/24, 05/30, 06/02, 07/03, 07/12, 07/23, 07/28, and 09/24; however, the technique used in this study did not recognize them (Figure 7). On 05/30, 07/03, 07/12, 07/23, and 07/28, however, this study detected a sea breeze that propagated inland and reached areas close to the SRS. The high correlation between these two independently performed sea breeze identification works with different methods and datasets – one using 10m wind and dew point temperature, satellite imagery and radar imagery, and the other using 61m wind, dew point temperature, air temperature, ceilometer backscatter, and radar – demonstrates that both approaches are robust and

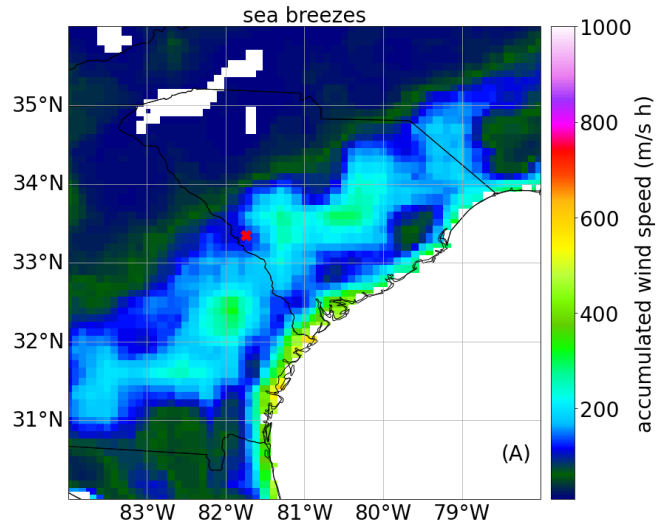


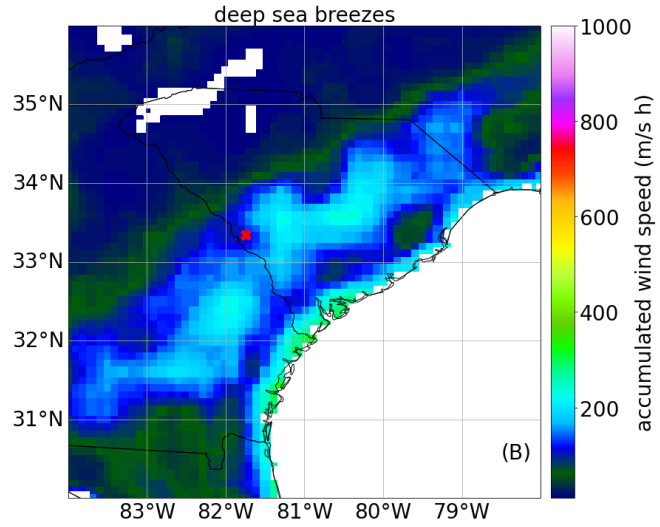


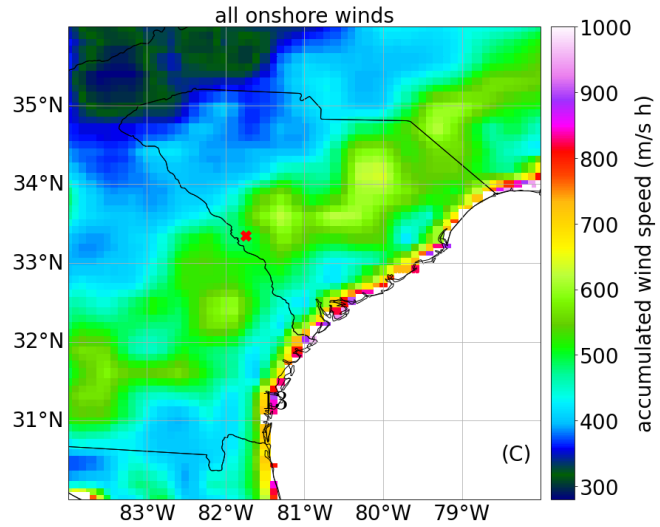


suitable for sea breeze

climatological investigations.

### 3.2 **Spatial distribution of sea breeze with winds**

Figure 8 shows a composite of sea breeze, aggregated over all sea breeze days from March 1 through September 30, 2019. Figure 8A included all identified sea breezes, regardless of how far inland they traveled. The pattern is clear: along the coastline, there is a narrow band of strong sea breeze onshore winds, with a maximum velocity of 600 (m/s h), and there is a high probability that the onshore wind will extend approximately 200 kilometers inland, in a band parallel to the coast. The sea breeze onshore wind is evenly distributed within this band, except for a few locations with higher values, indicating that the inland advecting sea breeze has a similar chance of reaching any location within the band. The SRS is located close to the boundary zone of this band, after which the onshore wind quickly weakened. The average values of the accumulated sea breeze winds in this band range between 150 and 300 m/s h. There is still some residue accumulation of winds further inland, but it is unclear whether these are inland penetrating sea breeze winds or winds brought in by other mechanisms during the sea breeze identification phase.

Figure 8B only includes the sea breezes that propagate deep inland. The wind band in Figure 8B has nearly the same magnitude and distribution as in Figure 8A. Figure 8B demonstrates that near the coast, inland-propagating sea winds are also stronger than onshore winds after moving inland. Figure 8C displays all onshore winds accumulated onshore, regardless of whether they are sea breeze winds caused by land-sea temperature difference. The total winds appear to be three times as much as those associated with deep inland sea breezes (Figure 8B) and twice as strong as in Figure 8A, as most areas in the sea breeze belt have a magnitude of about 200 m/s h in Figure 8A, 300 m/s h in Figure 8B, and 600 m/s h in Figure 8C.

Figure 8 depicts how sea breezes frequently propagate inland in the southeastern US coastal region, reaching around 160 km to and past the SRS. However, there appears to be a distinct boundary after which the accumulated sea breeze winds rapidly diminish (Figure 8A, B). The extent of the boundary decreases as latitude increases. The extent is more than 230 km in Georgia (latitude= [31-32]), about 210 km in South Carolina (latitude= [32-34]), and about 190 km in North Carolina (latitude>34). This boundary in Figure 8A and Figure 8B may represent a limit of the inland propagation of sea breeze in the southeast-ern United States. This result is consistent with the previous studies that showed the extent of inland penetration of sea breeze in mid-latitude regions (above 30o latitude) is normally less than 200km (Crosman and Horel 2010; Finkele et al. 1995; Miller et al. 2003).

### 3.3 **Modeling studies and theoretical estimate**

Figure 8B's Sea breeze propagation extent is further inland than many previously documented extents observed at mid-latitude (see Introduction). We conducted idealized and semi-idealized modeling experiments to investigate possible

causes of this discrepancy.

Experiment 1 used the WRF-ARW model (Skamarock et al. 2019). The physics schemes include WRF Dual Moment 5-class scheme Microphysics (Lim and Hong 2010), RRTMG scheme Long-wave and short-wave radiation (Iacono et al. 2008), Revised MM5 surface scheme (Jiménez et al. 2012); and Yonsei University Program PBL (Hong et al. 2006). The rectangle domain is a horizontal is 1200 km x 600 km with a grid spacing of dx=dy=3km. A virtual coastline is located at x=900km. There are 35 sigma vertical levels up to 190 hPa. A horizontally homogeneous initial condition used a weakly stable atmospheric sounding profile with an average Brunt Vaisala frequency of 0.0064 1/s from ground to 5 km (not shown). The RRTMG atmospheric radiation schemes simulate diurnal land temperatures between 17 and 30 °C, while the SST is 22 °C. Both the land and ocean surfaces have a zero-elevation ideal topography.

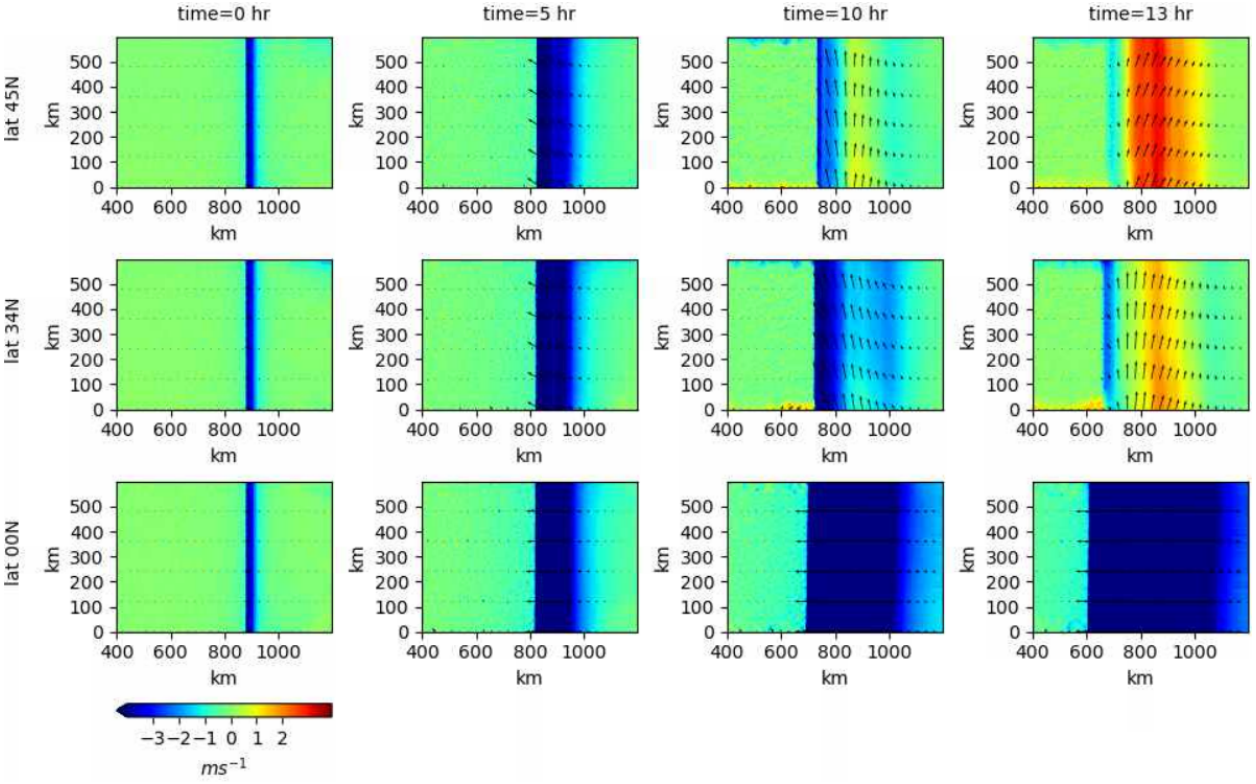


The experiment tested the sea breeze maximum inland propagation at latitude=0, 34°N, and 45°N under the idealized conditions described above. Figure 9 shows the results. Let t=0h be the start time for sea breeze winds, which have a 3 m/s westward onshore wind at x=900 km. At t=5h, onshore wind speeds are roughly the same for the three latitudes, but the Coriolis effect begins to turn the wind right at lat=34°N and lat=45°N. At t=10h, the winds shift to

the right and parallel to the virtual coastline at lat=34°N and lat=45°N. At lat=45°N, the wind blows northeast behind the leading front. Lat=0 has the farthest-reaching sea breeze winds, followed by lat=34°N and then lat=45°N. The leading front propagated about 170km inland for lat=34°N at t=10h. Observations between the leading front and the coast may indicate that the sea breeze has ended. Rotunno (1983) used a set of simplified linear equations of motion to derive and estimate the maximum extent of sea breeze inland propagation near the ground as $L = \frac{\mathrm{Nh}}{\sqrt{f^2-\omega^2}}$ for regions where the latitude is greater than 30° (i.e. $f > \omega$ ), where $f$ is the Coriolis parameter $f = 2\omega sin(\Phi)$ with $\omega$ being the latitude and $\omega$ the earth rotation angular speed of $2\pi$ per day, and $N$ is Brunt-Vaisala frequency that depicts the atmospheric stability, and $h$ is the vertical extent of the sea breeze winds. This distance agrees with Rotunno (1983)'s theoretical equation $L = \frac{\mathrm{Nh}}{\sqrt{f^2-\omega^2}}$ using N=0.0064 $f = 2\omega \sin 34$, and $\omega = \frac{2\pi}{\mathrm{day}}$, the ratio v/h=175, with v=1000 m (estimated as the height of the return flow, not shown) we have h=175km, about same as the modeled extent at t=10 h.

At t=13 h, most winds turn offshore (positive u) for lat=34°N and 45°N, but remain inland for lat= 0°. For lat=34°N, the inland-blowing leading front has detached from the rest of the wind field, which is now blowing northeast. For the purpose of mapping sea breeze's footprint, however, the leading front shown at t=13h should be included, even though the majority of the sea breeze event had already ended. The leading front's extent represents the maximum inland of an idealized sea wind simulation, as the front rapidly decreases after t=13h (not shown). At 13h for lat=45°N, the leading front winds are weaker than lat=0° and lat=34°N. For lat=34°N, at t=13h, the leading front extends approximately 220 km, which agrees with the mapping results shown in Figure 8, although uncertainty exists because, as previously stated, many factors are not considered in the idealized model experiment.

Experiment 2 is similar to Experiment 1 except that real topography and a varying latitude are used. The domain is 189 X 189 grid points with grid spacing dx=dy=3km. The terrain gradually rises going inland (not shown). The east-west u component and the north-south v component of the sea breeze are rotated by 45 degrees, so the negative values in Figure 10 represent the sea breeze wind blowing inland.

Within five hours after the sea breeze begins, a belt of 6 m/s inland sea breeze formed along the coast. For the next 15 hours, the sea breeze front moves inland. At t = 16 h, the inland wind belt begins to recede as some onshore winds shift offshore; thus t=15 h may represent the maximum inland propagation (Figure 10 C). Figure 10C and Figure 8 are similar with a maximum extent of 230 km in Figure 10 C and 225 km in Figure 8. Both Figure 10 C and Figure 8 show a reduction in the maximum extent from southwest to northeast. This is likely due to a stronger Coriolis force in the northeast portion of the domain where the wind directions became parallel to the coastline at t=15h and 16h, while

the winds are still toward onshore in the southwest corner. In Figure 8, coastal winds are higher than inland, similarly in Figure 10A at t=5h, the sea breeze wind belt near the coast is about 6m/s, stronger than at t=10 h, 15 h and 16 h.

Both Figure 10 C and Figure 8 show that the sea breeze propagates inland to about 230 km, which is larger than most observed extents in literature and also larger than the 175 km in Figure 9. In Figure 9 most sea breeze wind field shifted direction at t=13 h leaving only the leading front moving inland; whereas in Figure 10 C the majority of the sea breeze wind field is still inland at t=16h, with only the northeast corner starting to shift to offshore. This difference is likely because Figure 9 used flat elevation, whereas Experiment 2 used realistic topography, which enhanced convective air motion as well as sea breeze propagation. Figure 10 C and Figure 8 show a deeper sea breeze propagation than estimated using equations of Rotunno (1983) because they did not account for topography.

Figure 8 and Figure 10 can be compared because they both represent an averaged state of sea breeze propagation: Figure 8 shows the sum of sea breeze winds from March 1 to September 1, 2019, so the effects of different factors on different days are smoothed out; similarly, Figure 10 also represents the simulation of an idealized and thus averaged sea breeze propagation over a day because a horizontally uniform initial condition is realized with a single atmospheric sounding profile and zero initial wind, thus also smoothing out the possible effects of various factors that may appear on different dates in real simulations.

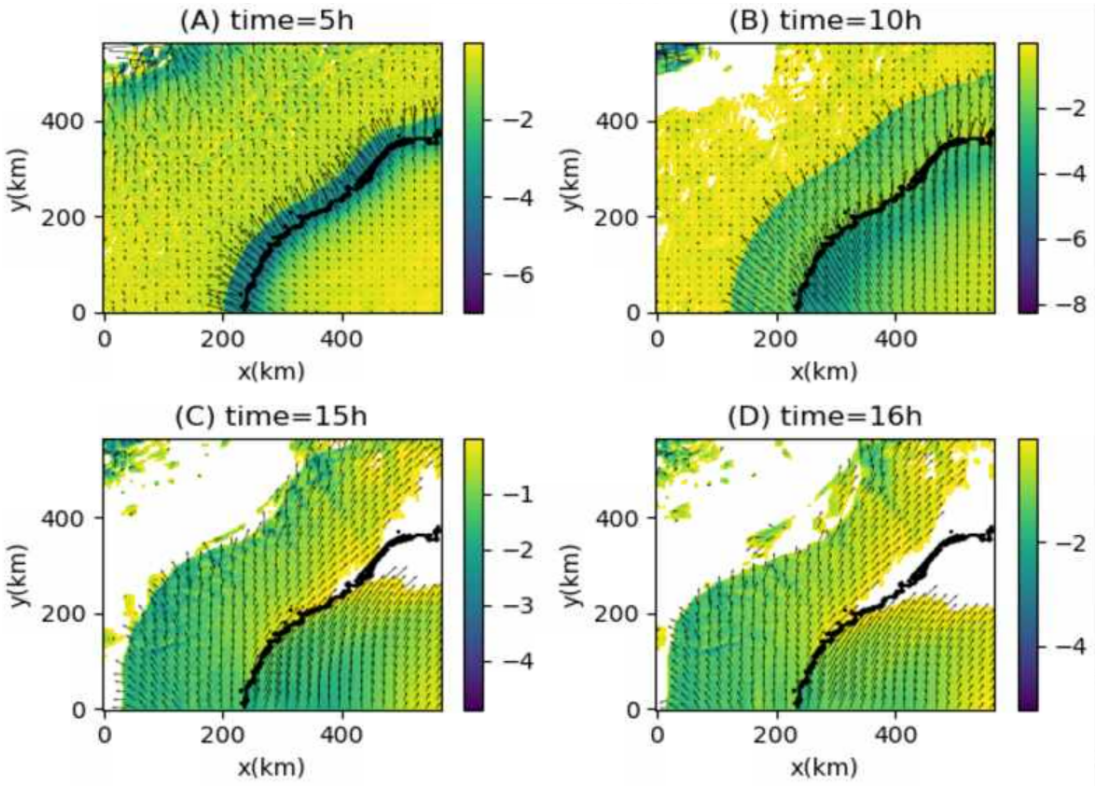


4 Conclusions

Using the ERA-5 surface re-analysis and remote sensing data, a scheme is developed to map the coastal regions of the South Eastern United States that are influenced by sea breeze onshore winds. The method identifies sea breezes based on changes in wind direction and dew point temperature, and then confirms them using cumuliform clouds in satellite imagery or coastal fronts indicated by cohesive lines in radar reflectivity. Additionally, filters are also used to eliminate onshore winds that are not caused by sea breezes. The scheme is demonstrated using a case study. The scheme's findings from March to September 2019 are compared with the results of a previous independent study conducted at the Savannah River Site, which revealed that the results of the two independent studies are highly consistent. From March to September 2019, this study identified 134 sea breeze days, a frequency of 63 percent. With the exception of June, which saw less sea breezes than May or July, sea breezes increased from March to July and then decreased. Onshore winds are strongest in a band near the coast. Deep inland propagation of sea breezes leaves footprints in a band parallel to the coastline with an inland distance of up to about 220 km, after which the sea breeze winds quickly diminish, indicating the limit of inland sea breeze propagation distance in the Southeastern United States. Idealized and semi-idealized WRF model experiments generated simulations that agree with the

mapping results. When a flat topography is used with the latitude=34°N, the sea breeze propagates inland reaching a distance of 175 km before most of the wind field shifts offshore leaving only a detached leading front still in the inland direction, which agrees with theoretical estimate. However, the areas that that detached leading front should be included in the mapping of sea breeze winds. When a realistic topography is used, a semi-idealized experiment simulated sea breeze that can propagate inland for a maximum of 230 km before retreating, consistent with the mapping result. Future studies are required to understand the sensitivities of sea breeze to a wide range of environmental variables.

There are limitations of this study that bring uncertainties. One of the uncertainties in this study is sometimes both sea breeze and synoptic scale storms happen at the same time. The identified surface sea breeze wind footprint may have included both effects, thus under such scenarios we may have overestimated the on-shore sea breeze wind by including the other synoptic effect, an issue that is not easy to solve. For example, (Qian et al. 2021) found that there are six circulation-based daily weather types in the warm season (March to October) in the SEUS, and sea breezes tend to occur in certain weather types more frequently than in others. Therefore, in future studies, weather type classification may be included to address the associated uncertainties.

**Acknowledgments**

This work was supported by the Laboratory Directed Research and Development (LDRD) program within the Savannah River National Laboratory (SRNL). This document was prepared in conjunction with work accomplished under Contract No. 89303321CEM000080 with the U.S. Department of Energy (DOE) Office of Environmental Management (EM). Publisher acknowledges the U.S. Government license to provide public access under the DOE Public Access Plan (https://www.energy.gov/downloads/doe-public-access-plan). The data analysis was performed on high-performance computing facilities from Cheyenne (doi:10.5065/D6RX99HX) provided by NCAR's Computational and Information Systems Laboratory, sponsored by the National Science Foundation. This information may not be further distributed without written approval from SRNL.

**References**

1. Arritt, R. W., 1993: Effects of the large-scale flow on characteristic features of the sea breeze. *Journal of Applied Meteorology and Climatology*, **32**, 116–125.

2.

3.

4.

5.

6.
7.
8.
9.
10.
11.
12.
13.
14.
15.
16.
17.
18.
19.
20.
21.
22.
23.
24.
25.
26.
27.
28.
29.
30.
31.
32.
33.
34.
35.
36.

37. Azorin-Molina, C., and J.-A. Lopez-Bustins, 2008: An automated sea breeze selection technique based on regional sea-level pressure difference: WeMOi. *International Journal of Climatology*, **28**, 1681–1692, https://doi.org/10.1002/joc.1663.Borne, K., D. Chen, and M. Nunez, 1998: A method for finding sea breeze days under stable synoptic conditions and its application to the Swedish west coast. *International Journal of Climatology*, **18**, 901–914.Buckley, R. L., and R. J. Kurzeja, 1997: An observational and numerical study of the nocturnal sea breeze. Part II: Chemical transport. *Journal of Applied Meteorology*, **36**, 1599–1619.Charabi, Y., A. Al-Bulooshi, and S. Al-Yahyai, 2013: Assessment of the impact of the meteorological meso-scale circulation on air quality in arid subtropical region. *Environ Monit Assess*, **185**, 2329–2342, https://doi.org/10.1007/s10661-012-2712-z.Crosman, E. T., and J. D. Horel, 2010: Sea and Lake Breezes: A Review of Numerical Studies. *Boundary-Layer Meteorol*, **137**, 1–29, https://doi.org/10.1007/s10546-010-9517-9.Finkele, K., J. M. Hacker, H. Kraus, and R. A. Byron-Scott, 1995: A complete sea-breeze circulation cell derived from aircraft observations. *Boundary-layer meteorology*, **73**, 299–317.Garratt, J. R., 1985: The inland boundary layer at low latitudes. *Boundary-layer meteorology*, **32**, 307–327.Goodman, S. J., and Coauthors, 2012: The GOES-R Proving Ground: Accelerating user readiness for the next-generation geostationary environmental satellite system. *Bulletin of the American Meteorological Society*, **93**, 1029–1040.Hadi, T. W., T. Horinouchi, T. Tsuda, H. Hashiguchi, and S. Fukao, 2002: Sea-Breeze Circulation over Jakarta, Indonesia: A Climatology Based on Boundary Layer Radar Observations. *Monthly Weather Review*, **130**, 2153–2166, https://doi.org/10.1175/1520-0493(2002)130<2153:SBCOJI>2.0.CO;2.Hong, S.-Y., Y. Noh, and J. Dudhia, 2006: A new vertical diffusion package with an explicit treatment of entrainment processes. *Monthly weather review*, **134**, 2318–2341.Hu, X.-M., and M. Xue, 2016: Influence of Synoptic Sea-Breeze Fronts on the Urban Heat Island Intensity in Dallas–Fort Worth, Texas. *Monthly Weather Review*, **144**, 1487–1507, https://doi.org/10.1175/MWR-D-15-0201.1.Hughes, C. P., and D. E. Veron, 2018: A Characterization of the Delaware Sea Breeze Using Observations and Modeling. *Journal of Applied Meteorology and Climatology*, **57**, 1405–1421, https://doi.org/10.1175/JAMC-D-17-0186.1.Iacono, M. J., J. S. Delamere, E. J. Mlawer, M. W. Shephard, S. A. Clough, and W. D. Collins, 2008: Radiative forcing by long-lived greenhouse gases: Calculations with the AER radiative transfer models. *Journal of Geophysical Research: Atmospheres*, **113**.Jiménez, P. A., J. Dudhia, J. F. González-Rouco, J. Navarro, J. P. Montávez, and E. García-Bustamante, 2012: A revised scheme for the WRF surface layer formulation. *Monthly weather review*, **140**, 898–918.Khan, B., Y. Abualnaja, A. M. Al-Subhi, M. Nellayaputhenpeedika, M. Nellikkattu Thody, and A. P. Sturman, 2018: Climatology of sea breezes along the Red Sea coast of Saudi Arabia. *International Journal of Climatology*,

**38**, 3633–3650.Koch, S. E., and C. A. Ray, 1997: Mesoanalysis of Summertime Convergence Zones in Central and Eastern North Carolina. *Weather and Forecasting*, **12**, 56–77, https://doi.org/10.1175/1520-0434(1997)012<0056:MOSCZI>2.0.CO;2.Kondo, H., 1990: A numerical experiment of the" Extended Sea Breeze" over the Kanto Plain. *Journal of the meteorological Society of Japan. Ser. II*, **68**, 419–434.Kottmeier, C., P. Palacio-Sese, N. Kalthoff, U. Corsmeier, and F. Fiedler, 2000: Sea breezes and coastal jets in southeastern Spain. *International Journal of Climatology: A Journal of the Royal Meteorological Society*, **20**, 1791–1808.Kozo, T. L., 1982: An Observational Study of Sea Breezes Along the Alaskan Beaufort Sea Coast: Part I. *Journal of Applied Meteorology and Climatology*, **21**, 891–905, https://doi.org/10.1175/1520-0450(1982)021<0891:AOSOSB>2.0.CO;2.Laird, N. F., D. A. R. Kristovich, X.-Z. Liang, R. W. Arritt, and K. Labas, 2001: Lake Michigan Lake Breezes: Climatology, Local Forcing, and Synoptic Environment. *Journal of Applied Meteorology and Climatology*, **40**, 409–424, https://doi.org/10.1175/1520-0450(2001)040<0409:LMLBCL>2.0.CO;2.Lim, K.-S. S., and S.-Y. Hong, 2010: Development of an effective double-moment cloud microphysics scheme with prognostic cloud condensation nuclei (CCN) for weather and climate models. *Monthly weather review*, **138**, 1587–1612.Lyons, W. A., 1972: The climatology and prediction of the Chicago lake breeze. *Journal of Applied Meteorology and Climatology*, **11**, 1259–1270.McKendry, I., and N. Roulet, 1994: Sea breezes and advective effects in southwest James Bay. *Journal of Geophysical Research: Atmospheres*, **99**, 1623–1634.Miller, S. T. K., B. D. Keim, R. W. Talbot, and H. Mao, 2003: Sea breeze: Structure, forecasting, and impacts. *Reviews of Geophysics*, **41**.Muñoz-Sabater, J., and Coauthors, 2021: ERA5-Land: A state-of-the-art global reanalysis dataset for land applications. *Earth System Science Data Discussions*, 1–50.Papanastasiou, D. K., D. Melas, and I. Lissaridis, 2010: Study of wind field under sea breeze conditions; an application of WRF model. *Atmospheric Research*, **98**, 102–117.Pearce, R. P., 1955: The calculation of a sea-breeze circulation in terms of the differential heating across the coastline. *Quarterly Journal of the Royal Meteorological Society*, **81**, 351–381.Qian, J.-H., B. Viner, S. Noble, and D. Werth, 2021: Precipitation Characteristics of Warm Season Weather Types in the Southeastern United States of America. *Atmosphere*, **12**, 1001, https://doi.org/10.3390/atmos12081001.Rotunno, R., 1983: On the linear theory of the land and sea breeze. *Journal of atmospheric sciences*, **40**, 1999–2009.Ryznar, E., and J. S. Touma, 1981: Characteristics of true lake breezes along the eastern shore of Lake Michigan. *Atmospheric Environment (1967)*, **15**, 1201–1205.Schwartz, M., 2006: *Encyclopedia of Coastal Science*. Springer Science & Business Media,.Simpson, J. E., 1994: *Sea Breeze and Local Winds*. Cambridge University Press,.Simpson, J. E., D. A. Mansfield, and J. R. Milford, 1977: Inland penetration of sea-breeze fronts. *Quarterly Journal of the Royal Meteorological Society*, **103**, 47–76, https://doi.org/10.1002/qj.49710343504.Skamarock, W. C.,

and Coauthors, 2019: A description of the advanced research WRF model version 4. *National Center for Atmospheric Research: Boulder, CO, USA*, **145**, 145.Viner, B., S. Noble, J.-H. Qian, D. Werth, P. Gayes, L. Pietrafesa, and S. Bao, 2021: Frequency and Characteristics of Inland Advecting Sea Breezes in the Southeast United States. *Atmosphere*, **12**, 950, https://doi.org/10.3390/atmos12080950.Wermter, J., S. Noble, and B. Viner, 2022: Impacts of the Thermal Gradient on Inland Advecting Sea Breezes in the Southeastern United States. *Atmosphere*, **13**, 1004, https://doi.org/10.3390/atmos13071004.

**Figure Captions**

Figure 1 The study domain is shown as the red box. The color shade shows the accumulated hourly onshore wind speed (in m/s h) for the detected sea breeze occurrence areas for the demonstration case between the local time of 12pm, May 18 to 12pm, May 19, 2019. The red cross represents SRS. To highlight the strong sea breeze areas, the color bar shows only accumulated winds $> 20$ m/s h

Figure 2 Flowchart of the steps to identify the sea breeze winds.

Figure 3 the cumulus clouds associated with a sea breeze occurrence on May 18, 2019, late afternoon at 20:00 UTC (16:00 local time), as recorded by GOES-16 satellite True Color display of visible channels. The blue line that separates cumulus clouds with a cloud-free belt near the coastline is a signature feature of sea breezes.

Figure 4 NEXRAD composite Radar reflectivity for late afternoon on May 18, 2019. Data source: NEXLAB at College of DuPage archived by National Centers for Atmospheric Research (NCAR).

Figure 5 GOES-16 satellite True Color display of visible channel on May 18, 2019, early afternoon at 15:00 UTC (11:00 local time)

Figure 6 Monthly distribution of the sea breeze occurrence in Southeastern US from March to September of 2019. Red shows all the identified cases, and the blue shows only the inland-propagation cases. Y-axis denotes the number of sea breeze occurrence.

Figure 7 Time-aggregated sea breeze winds (in m/s h) mapped in this study on the days when sea breeze winds are identified at SRS (red cross) by Viner (2021).

Figure 8 spatial distribution of the onshore sea breeze wind speed accumulated March-September 2019. (A) all identified sea breezes; (B)only identified sea breezes that propagated deep inland and (C) all onshore wind regardless of whether they are driven by thermal differences (so the synoptic scale storms are included).

Figure 9 idealized WRF simulation of sea breeze inland propagation at latitude=0 (top), 34N (middle) and 45N (bottom). Color indicates wind speed.

Positive wind is offshore and negative onshore. The arrows depict the wind direction. Coastline is located at x=900 km.

Figure 10 WRF sea breeze simulation in a semi-idealized configuration. The domain resembles that in Figure 1. Realistic elevation data is used. The color indicates cross-shore wind speed, and the arrows depict wind directions. Coastline is shown as the black curve. Only onshore winds are shown, and the offshore winds or non-wind areas are shown as blank. The times show the number of hours that have passed since the sea breeze begins